On the sensitivity of the instantaneous dimension of dynamical dystems and its insights on sea surface temperature anomaly field over the tropical Pacific

Ming Shi[1], Huang Yu[2,3], Zuntao Fu[4]*, Hao Xue[1], Xiaolong Qiu[1], Xintong Hao[1], Xiaohan Zhang[5], Haiyang Yu[5], Weiqi Xing[6]

[1]Renewable Energy Survey and Design Department, Huaneng Clean Energy Research Institute, Beijing,102209, China
[2]Munich Climate Center and Earth System Modelling Group, Department of Aerospace and Geodesy, TUM School of Engineering and Design, Technical University of Munich, 80333, Germany.
[3]Complexity Science, Potsdam Institute for Climate Impact Research, Potsdam, 14412, Germany
[4]Laboratory for Climate and Ocean-Atmosphere Studies, Department of Atmospheric and Oceanic Sciences, School of Physics, Peking University, Beijing, 100871, China
[5]Engineering Department, China Huaneng Group Corporation Limited, 070001, China
[6]Qinghai Branch of China Huaneng Group Corporation Limited, 810008 , China

Correspondence to: Zuntao Fu (fuzt@pku.edu.cn), Ming Shi (m_shi@qny.chng.com.cn)

Abstract. Sea surface temperature anomaly (SSTA) fields over the tropical Pacific exhibit complex spatiotemporal variability that traditional regional average indices may fail to capture. In this study, we take the evolution of daily SSTA fields as a dynamical system (DS) and compute the DS instantaneous dimension (DSID) to characterize local dynamical properties. Our results reveal a significant shift in the mean value (SMV) of DSID around the year 2007 over the western tropical Pacific (notably the Niño 4 and Niño 3.4 regions), a phenomenon that is absent in the eastern Pacific.To explain this region-dependent SMV of DSID in SSTA fields, we examine the sensitivity of DSID to the changes of the system states using idealized system models, such low-dimensional (Lorenz-63) and high-dimensional (Lorenz-96) systems. Results demonstrate that the estimation of DSID is sensitive to variations in both high-frequency variability and system states,for both low-dimensional and high-dimensional systems. These findings from idealized systems provide a theoretical basis for interpreting the observed SMV in SSTA fields. Further analysis reveals that the SMV in DSID can be largely attributed to changes in high-frequency variability across different time spans. Collectively, these results advance our understanding of the physical interpretation of DSID and offer valuable insights for the study of complex real-world systems.

Keywords:

Instantaneous dimension, sensitivity, Lorenz system, sea surface temperature anomalies, high-frequency variability, SMV

1 Introduction

As one of the most studied sub-units in the climate system, sea surface temperature (SST) of tropical Pacific plays a critical role in impacting climate variations and variability. SST varies across a wide range of temporal and spatial scales

(Deser and Blackmon, 1993; Kushnir, 1994; Wu and Liu, 2005; Fan and Schneider, 2012; Strobach et al, 2020; Girishkumar et al, 2021), which is confirmed by the observed spectra for tropical SST with the dominated structures from intraseasonal to interdecadal time scales (Kug et al, 2009) related to the El Niño-Southern Oscillation (ENSO). The usual way quantifying El Niño event is to use some simple indices defined by averaging SST anomalies (SSTA) or from the empirical orthogonal decomposition coefficient of SSTA over some specific regions (Ashok et al, 2007; Kug et al, 2009; Kao and Yu, 2009; Jeong and Ahn, 2017), such as Niño 3 index from Niño 3 region (5°N-5°S, 150°W-90°W), Niño 4 index from Niño 4 region (5°N-5°S, 160°E-150°W), Niño 3.4 index from Niño 3.4 region (5°N-5°S, 170°W-120°W). However, such definition based on the regional average or regional decomposition of SSTA may miss some important features of SSTA field (Trenberth and Stepaniak, 2001), such as the gradients of regional averaged SST anomalies quantified by Trans-Niño index (TNI, defined as difference of the regional averaged SSTA between Niño 1+2 region (0°-10°S, 90°-80°W) and Niño 4 region). Moreover, SSTA variability is not limited only to the ENSO events. Marine heat waves (MHW), which are episodes of anomalous warm SSTA with timescales from days to months (Lima and Wethey, 2012; Frolicher and Laufkotter, 2108; Oliver et al, 2018; Holbrook et al, 2019), and coastal upwelling for episodes of anomalous cold SSTA lasting weekly (Kämpf et al, 2004; Hu et al, 2021; Huang et al, 2022b), are two severe ocean extreme events. Actually, the evolution of all these SST anomalies from a wide range of scales over a given region can be taken as a dynamical system. For example, Vallis developed a conceptual model of El Niño by modelling El Niño as a low-dimensional chaotic system (Vallis, 1986 and 1988), which can be further transformed into the classical Lorenz-63 model (Garay and Indig, 2015; Borghezan and Rech, 2017). And results from both simple low-order chaotic process and complicated climate models suggest that ENSO features are consistent with the low-order chaotic behavior (Tziperman et al, 1994; Jin et al, 1994).

Several methods have been proposed to characterize the dynamical properties of systems. Ding and Li (2007) proposed the nonlinear local LE (NLLE) method to study predictability of the dynamical system. This method accounts for nonlinear error growth of a finite size, and has been widely used in studies of atmospheric predictability (Li and Ding, 2011; Feng et al., 2014, 2018; Ding et al., 2015; Hou et al., 2018, 2022; Li et al., 2020a; He et al., 2021). Li et al. (2019) proposed the backward NLLE (BNLLE) method, based on the NLLE method, which is applicable to studies of the predictability of extreme events (Li and Ding, 2023). Li et al. (2017) introduced the attractor radius (AR) and global AR (GAR) to depict the geometric characteristics and average behavior of chaotic systems. These two statistics can quantify the predictability limits of chaotic systems from the geometric characteristics and average behavior of error growth, and have been applied to the predictability of extreme weather or climate events (Li et al., 2023). However, these methods focus primarily on the predictability of dynamical systems and do not explore the dynamical properties of the system from other perspectives.

Recently, Lucarini, Faranda, and their collaborators developed a method based on dynamical systems and extreme value theory to characterize the instantaneous dynamical properties of a given system, which is referred to as the dynamical systems (DS) method (Lucarini et al., 2012; Faranda et al., 2017a and 2017b).This method reconstructs the attractor of the dynamical system using the system trajectory $X(t)$, and computes two dynamical parameters—the instantaneous dimension $d(\zeta)$ and the instantaneous persistence parameter $\theta(\zeta)$ — to characterize the instantaneous dynamics of a given climate

system. The instantaneous dimension $d(\zeta)$ measures the degree of divergence of the attractor trajectories in the neighborhood of time $t = \zeta$ in phase space, and is related to the local number of degrees of freedom of the dynamical system. The instantaneous persistence parameter $\theta(\zeta)$, defined as the inverse of the persistence, quantifies the strength of persistence of the attractor in the vicinity of time $t = \zeta$. This method provides an alternative perspective for understanding the behavior of dynamical systems. Faranda and his collaborators (Faranda et al, 2017a) have interpreted the physical meaning of the DS instantaneous dimension (DSID) and inverse of persistence in some idealized systems, such as Lorenz system (Lorenz, 1963). They found that the instantaneous dimension of the low-dimensional systems can provide a direct way to compute the dimensions of the attractor without embedding (Faranda et al, 2017a), and the calculated minima and maxima of the instantaneous dimension are able to track the extremes of the Lorenz attractor.

DS method has been employed to a wide range of fields, such as studies on the mid-latitude weather extremes (Messori et al, 2017), atmospheric circulation (Sun et al, 2022), atmospheric predictability (Faranda et al, 2019, Dong at al.,2025), compound climate extremes (Luca et al, 2020a and 2020b; Faranda et al, 2020) and climate effects of ENSO (Franda et al., 2025). And by taking the evolution of SSTA field over a specific region as a DS, its corresponding instantaneous dimension and inverse of persistence can provide more information than those from the averaged SSTA (Huang et al, 2022a; Shi et al, 2022; Guo et al, 2022; Huang et al, 2022b; Huang and Fu, 2019).It is obvious that there is a marked shift in the mean value (SMV) of DSID, which is defined as distinguishable mean value difference of DSID between two intervals over a given region, (Details for its calculation can be found in the subsection of 2.3 Dynamical Systems parameters) over only some regions, but not discernible over others (Fig. 1). What are the reasons for this marked SMV of DSID over some preferred regions (such as Niño 3.4 or Niño 4 in Fig. 1c and 1d) and predominant difference among different regions? Is it related to the sensitivity of DSID to any factors?

To answer these problems, we may find some clues by analyzing the sensitivity of DSID to some specific factors from the idealized Lorenz system, since the physical meaning of DSID and inverse of persistence have been interpreted with this idealized system. It should be pointed out that all results related to this idealized system are free from the noise. However, the measurement noise is inevitable for observations from the real-world systems. Although there are some theoretical and numerical studies on effects of observational noise or stochastic perturbations on extreme value law or dimension of systems (Faranda et al, 2013; Faranda and Vaieti, 2014, Faranda et al, 2016), the robustness of computed DSID to the noise and more other factors has not been well explored, especially about the real-world systems.

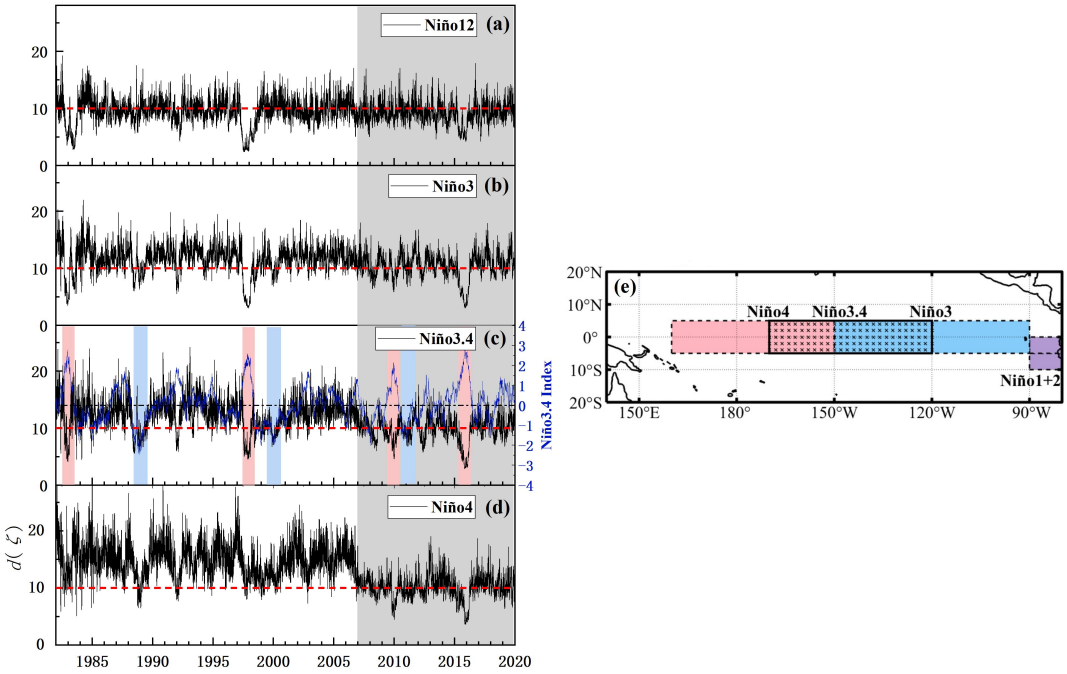

Figure 1: The evolution of calculated instantaneous dimension d of daily sea surface temperature anomalies over four typical Niño regions. (a) Niño1+2, (b) Niño 3, (c) Niño 3.4, (d) Niño 4. The blue curve in (c) represents Niño3.4 index. Shading denotes the typical El Niño events (red) and La Niña events (blue). The gray shaded area represents the periods after 2007. Red dashed lines are eye guides for the variation of the DSID mean value. (e) The geographical locations of the four Niño regions: Niño1+2 region (0°-10°S, 90°-80°W), Niño3 region (5°N-5°S, 150°W-90°W), Niño3.4 region (5°N-5°S, 170°W-120°W) and Niño4 region (5°N-5°S, 160°E-150°W) .

The rest of this paper is organized as follows. Section 2 describes the SST data and related methods used in this study. Section 3 presents the detailed results on the idealized Lorenz systems, especially the sensitivity of DSID to two kinds of factors, measured noise and changes of system states. Section 4 shows the evolution of the calculated DSID over different tropical Pacific regions where SMV of DSID is revealed and possible explanations are provided. Companied with the SMV of DSID and its causes, some possible impacts on related studies are discussed. At last, a summary is given in Section 5.

2 Data and Methods

2.1 Data

The daily SST data from 1982 to 2019 is retrieved from National Oceanic and Atmospheric Administration (NOAA), and it is 1/4° daily Optimum Interpolation SST version 2 (dOISST.v2) high-resolution blended analysis of SST based on

infrared satellite observations (Reynolds et al, 2007; Banzon et al, 2016). To reduce the potential influences from the periodic and long-term warming trend, the long-term climatological average for each calendar day over all of years and the linear trend fitted by least square over the whole span are removed to derive the anomalies for computing DS parameters, both the instantaneous dimension and the inverse of persistence.

2.2 Lorenz system

To explore the sensitivity of DSID to different factors, the idealized model, Lorenz system (Lorenz-63) (Lorenz, 1963) is adopted, following the work of Faranda and his collaborators (Faranda et al, 2017a). The classical Lorenz-63 system is defined as follows

$$\begin{cases} \frac{dx}{dt} = a(y - x) \\ \frac{dy}{dt} = rx - y - xz \\ \frac{dz}{dt} = xy - bz \end{cases} \quad (1)$$

with the system parameters $a = 10, b = \frac{8}{3}, r = 28$ for typical chaotic regime. By the 4th-order Runge-Kutta method, Eq. (1) can be numerically solved with a time step of 0.025 to generate its trajectory $\boldsymbol{X}(t) = \{x(t), y(t), z(t)\}$ in phase space.

To confirm the sensitivity of DSID to noise is not limited only to the low-dimensional system, similar test is also carried on a higher-dimensional system by using a 40-dimensional Lorenz 96 (Lorenz-96) model (Lorenz, 2006). Each degree of freedom x_i in the model evolves according to the following local interactions

$$\frac{dx_i}{dt} = (x_{i+1} - x_{i-2})x_{i-1} - x_i + F \quad (2)$$

with periodic boundary conditions. We set $F = 8$ and numerical integration is performed with a time step $\Delta t = 0.05$.

2.3 Dynamical Systems parameters

DS method takes the evolution of a given spatial-temporal field to be a dynamical system, and an observed phase-space trajectory $\boldsymbol{X}(t)$ can approximate the temporal evolutions of the states of this dynamical system. For example, $\boldsymbol{X}(t)$ can be the trajectory $\boldsymbol{X}(t) = \{x(t), y(t), z(t)\}$ in phase space for Lorenz-63 system, a reference point $\boldsymbol{\zeta}$ for a specific time t_0 on this trajectory would be a given point $(x(t_0), y(t_0), z(t_0))$. Taking SSTA as an example, $\boldsymbol{X}(t)$ is a vector sequence of daily SSTA latitude-longitude maps, a reference point $\boldsymbol{\zeta}$ on this trajectory would be a SSTA latitude-longitude map for a specific day (Huang et al, 2022b; Shi et al, 2022).

In order to describe an instantaneous state around a reference point $\boldsymbol{\zeta}$ and measure the dynamical properties of the given system near this point $\boldsymbol{\zeta}$, a distance function is defined by $g(\boldsymbol{X}(t), \boldsymbol{\zeta}) = -\log[\mathrm{dist}(\boldsymbol{X}(t), \boldsymbol{\zeta})]$, in which "dist" denotes a Euclidean distance between $\boldsymbol{\zeta}$ and each point on the trajectory $\boldsymbol{X}(t)$. By this way, $g(\boldsymbol{X}(t), \boldsymbol{\zeta})$ can sort out the points on the trajectory $\boldsymbol{X}(t)$ most close to $\boldsymbol{\zeta}$. For a given threshold s, such as the top 2% percentile (the quantile threshold $p = 0.98$) of $g(\boldsymbol{X}(t), \boldsymbol{\zeta})$, all points of the exceedances $u(t, \boldsymbol{\zeta}) = g(\boldsymbol{X}(t), \boldsymbol{\zeta}) - s$ (without taking $u(t, \boldsymbol{\zeta}) < 0$ into account) form a group of all

analogues of ζ on the trajectory. And the cumulative probability distribution (CDF) of $u(t, \zeta)$ follows the Generalized Pareto Distribution (GPD) function (Lucarini et al, 2012; Faranda et al, 2017a) as:

$$P(u, \zeta) \simeq \exp\left[-\theta(\zeta)\frac{u(\zeta)}{\sigma(\zeta)}\right] \quad (3)$$

with two DS parameters $d(\zeta) = 1/\sigma(\zeta)$ and $\theta(\zeta)$. $d(\zeta)$ is a parameter related to the instantaneous dimension and $\theta(\zeta)$ related to the inverse of the mean residence time at ζ (dynamical persistence parameter) (Faranda et al, 2017a; Faranda et al, 2017b; Messori et al, 2017). Since each point ζ on $\boldsymbol{X}$(t) can derive a certain value for $d(\zeta)$ or $\theta(\zeta)$, the computed results for all the time points will obtain the time series of instantaneous dimension and instantaneous persistence parameters, which are denoted by d(t) and θ(t). In this study, since θ(t) is not so sensitive to noise as d(t) (Figure not shown here) and detailed results about θ(t) have been reported (Shi et al, 2022), we focus on the sensitivity of d(t) and its application. It should be pointed out that ***the estimation of DSID is calculated over the whole span.*** Datseris et al.(2023) discused the caveats of this methodology: (1) The choice of quantile threshold p should satisfy the condition that N(1 - p) $\geqslant$ 100-1000 (N is the data length), to ensure that the number of exceedances is sufficient for a reliable fit. And the p should satisfy the NRMSE test. (2) There does not exist a method (visual or statistical) in the literature that can confidently falsify this approach, nor that it can quantify its significance meaningfully. Further research is needed in this regard. To assess the robustness of our results, we added a sensitivity analysis on the choice of quantile thresholds (5% and 1%, i.e., p = 0.95 and p = 0.99); see the Supporting Information for details. We conclude that the selection of the quantile threshold does not affect the findings of this study.

2.4 Significance test on SMV of DSID

From the results shown in Fig. 1, it is obvious that there may exist a mark shift, mean value or standard deviation, for the estimation of DSID. In order to test whether this shift is significant or not, we employ the block bootstrap method for statistical testing considering strong autocorrelation in the DSID time series. The bootstrap method (a resampling technique) was proposed by Efron in 1979 (Efron, 1992). Its principle is to conduct repeated sampling with replacement from the original data, thereby increasing the sample size and facilitating the estimation of parameters and confidence intervals.The classical bootstrap method assumes that the data are independent and identically distributed.(i.i.d.) (Efron, 1992). However, for data with autocorrelation, directly resampling individual points would disrupt their inherent structure, resulting in biased estimations. The block bootstrap method can solve this problem.The procedure is as follows: the data are divided into blocks, the blocks are resampled with replacement, and the resampled blocks are then concatenated to form a new sequence. The dependency characteristics of the original sequence can be completely preserved within each block in this way. Depending on the different block partitioning methods, it can be classified into the moving block bootstrap (MBB) (Künsch, 1989), the non-overlapping block bootstrap (NBB) (Hall, 1985; Carlstein, 1986), and the stationary bootstrap (SB) (Politis and Romano, 1994).

We employ the most commonly used moving block bootstrap (MBB) method for statistical testing and determine the block length l using the Hall–Horowitz–Jing method (Hall at al., 1995). The specific steps are as follows. We generated 1000

pseudo-sequences using the MBB method to estimate the DSID. Then we have tested the significance of all results by repeatedly calculating the mean values or standard deviation of the estimated DSID over two periods separated by a break found in Fig. 1 or other figures. From 1000 calculated DSID differences, we can obtain the confidence intervals at a given significance level. By this way, all resulted SMV of DSID found in this study are significant at the 0.001 level.

3 Instantaneous dimension and its sensitivity in Lorenz systems

3.1 Instantaneous dimension and the effect of noise

Figure 2a shows the temporal evolution of the instantaneous dimension from the Lorenz-63 system with the classical chaotic parameter setting. The average value of DSID is close to the asymptotic mean of d (2.06), which is the theoretical value of dimension of the Lorenz attractor reported in the literature (see Faranda et al, 2017a; Faranda et al, 2017b; Messori et al, 2017 and references therein). It is also obvious that the values of the DSID fluctuate largely around this asymptotic mean with a range from 1.59 to 3.65 due to different states. The asymptotic mean of DSID only quantifies the global mean dimension of the attractor, not the local details of the attractor, let alone the transitions among different states. The details of DSID evolution also show that the local extreme values of the DSID, high or low, always appear in clusters and they track the extremes of Lorenz attractor (Faranda et al, 2017a). These results indicate that the DSID can indeed capture the detailed evolution features of Lorenz attractor, including the transitions among different states, such as extremes and non-extremes.

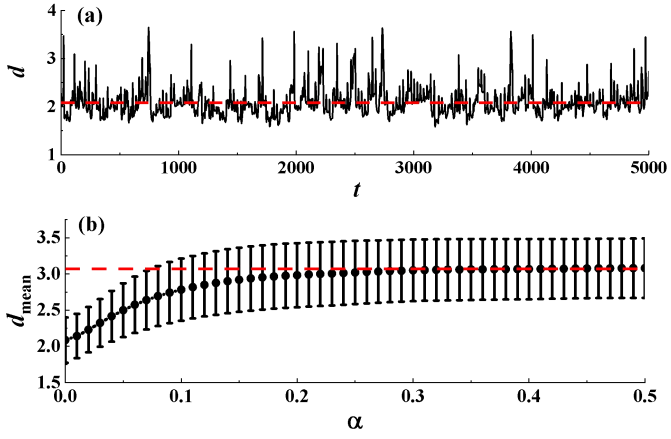

Figure 2 : (a) Time series of calculated instantaneous dimension d from Lorenz-63 system (with a time step Δt=0.025, data length N=5000). The red line denotes the asymptotic mean of d (2.06). (b) The variation of mean (dots) and standard deviation (bars) of d with the noise intensity α from noise-corrupted Lorenz-63 system. The red line for the asymptotic mean of d (3.08).

The above results are from noise-free Lorenz-63 system, however, the measurement noise is inevitable for observations from the real-world systems. It is necessary to check the effect of noise on the estimation of DSID. For this purpose, the noise-corrupted observations from Lorenz systems can be taken as

$$\boldsymbol{X}_{\mathbf{noise}}(t)=\boldsymbol{X}(t)+\alpha\boldsymbol{\varepsilon}(t) \quad (4)$$

where $\boldsymbol{X}(t)=\{x(t),y(t),z(t)\}$ is normalized output from noise-free Lorenz-63 system Eq. (1) or $\boldsymbol{X}(t)=\{x_i,i=1,...,k\}$ normalized output from noise-free Lorenz-96 system Eq. (2) with k its system dimension, $\boldsymbol{\varepsilon}(t)=\{\varepsilon_x(t),\varepsilon_y(t),\varepsilon_z(t)\}$ is Gaussian noise with zero mean and unit variance, α for the noise intensity. And $\boldsymbol{X}_{\mathbf{noise}}(t)$ is measured data with observational noise.

As expected, the mean values of DSID from the noise-corrupted Lorenz-63 system Eq. (4) increase with the enhancing noise intensity (Fig. 2b) when the noise intensity is not so strong. When the noise intensity reaches a critical value, such as 0.25, the mean values of DSID saturates to a dimension around 3.0, which is consistent with the previously reported studies (Faranda et al, 2013; Faranda and Vaienti, 2014; Faranda et al, 2016), where noise dominates the system and it makes the Lorenz-63 attractor difficult to detect.

Similar behaviors (Figure not shown here) can also be revealed in noise-free Lorenz-96 system Eq.(2) and noise-corrupted Lorenz-96 system Eq.(4). These results indicate that the estimation of DSID is sensitive to noise or high-frequency variability for both low-dimensional and high-dimensional systems.

3.2 Shift of instantaneous dimension and possible ways

Since the estimation of DSID is sensitive to noise or high-frequency variability for both low-dimensional and high-dimensional systems, this feature may be universal for all dynamical systems, partly as reported in the previous studies (Faranda et al, 2013; Faranda and Vaienti, 2014; Faranda et al, 2016). Then we can test whether we can reproduce the marked SMV of DSID found from SSTA field in Lorenz systems. The results in Fig. 2 suggest that there may exist the SMV of the estimated DSID when the system is dominated by different dynamics over different spans, such as from noise-free chaotic attractor to noise-corrupted chaotic attractor. Here we consider two possible routines in which the SMV of estimated DSID may take place.

The first one is the effect of noise, where the system follows

$$\boldsymbol{X}'(t)=\begin{cases}\boldsymbol{X}(t), 0\le t\le N/2\\ \boldsymbol{X}(t)+\alpha\boldsymbol{\varepsilon}(t), N/2\le t\le N\end{cases} \quad (5)$$

where $\boldsymbol{X}(t)$ and $\boldsymbol{\varepsilon}(t)$ are defined same as in Eq.(4), N for data length.

The estimated DSID from system Eq.(5) indeed can reproduce the regime-shift of DSID at the breaking point of N/2. For Lorenz-63 system, the mean values of DSID are 2.14 (noise-free) and 2.50 (noise-corrupted) before and after the breaking point of N/2 (N=8000 in this study) with different variances 0.36 and 0.83, respectively (Fig. 3a). From the temporal evolution of DSID, it is also obvious that there exist marked differences before and after the breaking point of N/2. The added noise destroys the ordinal patterns and enlarge the system dimension with more high-frequency variability.

Similar behaviors can also be reproduced in the Lorenz-96 system (Fig. 3c). These results indicate that observational noise or high-frequency variability indeed can induce the shift of DSID in both low-dimensional and high-dimensional systems.

The second case is a transition of states under a special system state, such as r=71.535, Lorenz-63 system is under the intermittent chaotic state (Manneville and Pomeau, 1979 and 1980), under which the evolution of system can change from chaotic state to periodic state even the system parameters unchanged. Similarly, the temporal evolution of the DSID is indeed able to capture this transition exactly, see Fig. 3b.

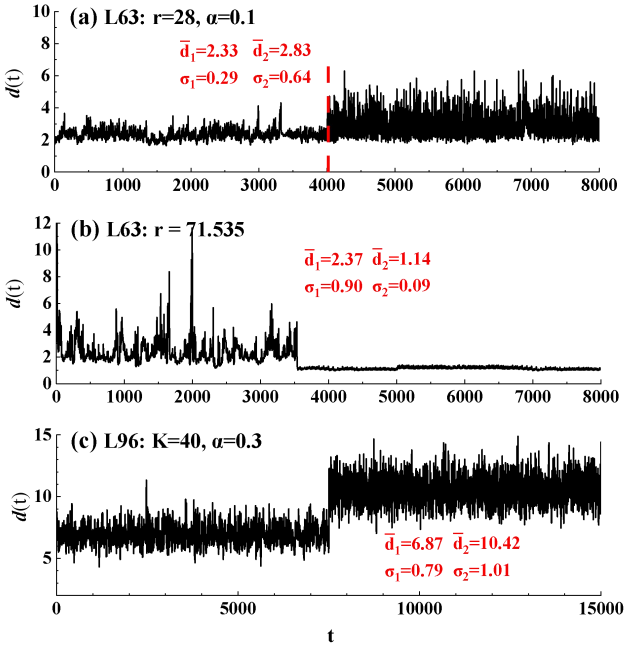

Figure 3: Shift of instantaneous dimension d from Lorenz systems. (a) Noise effect for Lorenz-63 system under chaotic state r=28: the first half is noise-free and the second half (after 4000) with α=0.1 random noise. (b) State changes for Lorenz-63 system under intermittent chaotic state r=71.535: the chaotic state transition to periodic state at t=3450. (c) Noise effect for Lorenz-96 system under chaotic state: the first half is noise-free and the second half (after 7500) with α=0.3 random noise. Both mean and standard deviation shifts of DSID are significant at the level of 0.001 from moving block bootstrap (MBB) test.

4 SMV of instantaneous dimension in SSTA over tropical Pacific and its causes and impacts

4.1 SMV of instantaneous dimension in SSTA over tropical Pacific

The distinguishable SMV of the DSID found in the SSTA field is with more complicated underlying dynamics (Fig. 1). First of all, when the typical ENSO events occur, the values of the DSID drop sharply. This result is consistent with the previous findings about the DSID that it can track the extremes of the underlying systems (Jin et al, 1994; Messori et al,

2017; Huang et al, 2022b, Shi et al, 2022), since both the El Niño and La Niña events are all extreme states of SSTA (Trenberth and Stepaniak, 2001; Ashok et al, 2007; Kug et al, 2009; Kao and Yu, 2009; Jeong and Ahn, 2017; Huang et al, 2022b). These sharp drops indicate that the spatial pattern of SST is relatively uniform at extreme states and can be described with fewer degrees of freedom in phase space. In contrast, when the SST is in neutral state, the DSID is higher, reflecting a more complex and irregular spatial pattern of SST. This phenomenon is consistent with observations. These sharp drops correspond to the situation of Lorenz systems dominated with low-frequency variability or quasi-periodic component.

Apart from these sharp drops over all studied regions, there is also a marked SMV of the DSID revealed around the year of 2007 from the temporal evolution of the calculated DSID over some specific regions, for example, Niño 3.4 region (Fig. 1c) and Niño 4 region (Fig. 1d). The details of statistics for the mean value and variance of the DSID before and after 2007 are summarized in **Table 1**, in which transitions of both mean value and variance are more predominant over both Niño 3.4 and Niño 4 regions.

Table 1 Statistics for the mean value and variance of the DSID before and after 2007, bold for significant at the level of 0.001 from moving block bootstrap (MBB) test.

	$\bar{d}$			σ^2		
	Before 2007	After 2007	$\bar{d}_{\mathrm{Diff}}$	Before 2007	After 2007	$\sigma^2{}_{\mathrm{Diff}}$
Niño 1+2	8.80	8.01	**-0.79**	5.39	3.79	**-1.60**
Niño 3	9.82	8.17	**-1.65**	4.43	2.49	**-1.94**
Niño 3.4	11.55	8.14	**-3.41**	8.11	2.66	**-5.45**
Niño 4	14.72	9.28	**-5.44**	12.33	3.98	**-8.35**

4.2 Possible causes of SMV of instantaneous dimension in SSTA over tropical Pacific

Different from the sharp drops of the DSID closely related with the typical ENSO events, the reasons for the SMV found around the year of 2007 are not easily determined. Inspired by the results from low-dimensional and high-dimensional Lorenz systems in section 3, we may conjecture that the major cause of this shift found around the year of 2007 is from the effect of the noise or high-frequency variability. To validate this conjecture, the contribution of the noise or high-frequency variability has to be filtered out from the raw SSTA. The simplest way is to make difference by defining the increment of the SSTA over each grid as follows

$$SSTA'_i(t) = SSTA_i(t+1) - SSTA_i(t) \tag{6}$$

where the subscript i denotes the specific grid.

Obviously, the high-frequency variability of SSTA indeed contributes differently over different Niño regions. The high-frequency variability is nearly indistinguishable by eye between before and after the year of 2007 over Niño 1+2 region. However, there are prominent differences in the high-frequency variability between these two periods over the Niño 3.4 and Niño 4 regions (Fig. 4a). The different contributions from the high-frequency variability of SSTA between two periods can be also revealed clearly in the scatter plot of their variance (Fig. 4c, black points), where the variance from Niño 1+2 region is the closest to the one-to-one diagonal line, but the largest deviation from Niño 4 region (Fig. 4c).

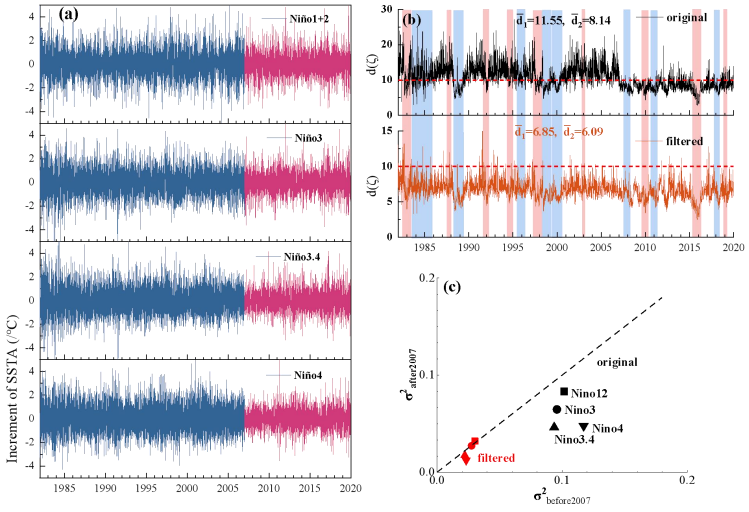

Figure 4: (a) The normalized increment series of daily SSTA averaged over four different Niño regions. The blue part denotes time series before 2007 and the pink part for after 2007. (b) The evolution of calculated instantaneous dimension *d* from the original (black) and 7-day low-pass filtered (blue) daily SSTA over Niño 3.4 region. (c) The scatter plot of variance of increment series before v.s. after 2007 from the original (black) and 7-day low-pass filtered (red) daily SSTA averaged over four different Niño regions with Niño 1+2 square, Niño 3 circle, Niño 3.4 up-triangle and Niño 4 down-triangle. Shifts for both DSID and increment of SSTA are significant at the level of 0.001 from moving block bootstrap (MBB) test for original data, filtered Niño 3.4 and Niño 4 data, but not significant for filtered Niño 1+2 and Niño 3 data.

To further confirm that the SMV of the DSID results from the high-frequency variability, we filter the SSTA for each grid over a specific region with 7-day low-pass Butterworth filter to remove the high-frequency variability lower than 7 days. Taking the results from Niño 3.4 region as an example, the marked SMV almost disappear after this filtering (see Fig. 4b), with the DSID difference before and after the year of 2007 changing from 3.41 to 0.76. This result indicates that the high-frequency variability difference before and after the year of 2007 is the major cause to induce the SMV of the DSID between two periods. Moreover, after 7-day low-pass filtering, the variances from different regions all lie along the one to one

diagonal line (Fig. 4c). These results further validate that the high-frequency variability difference between two periods contributes mainly to the SMV of DSID in SSTA.

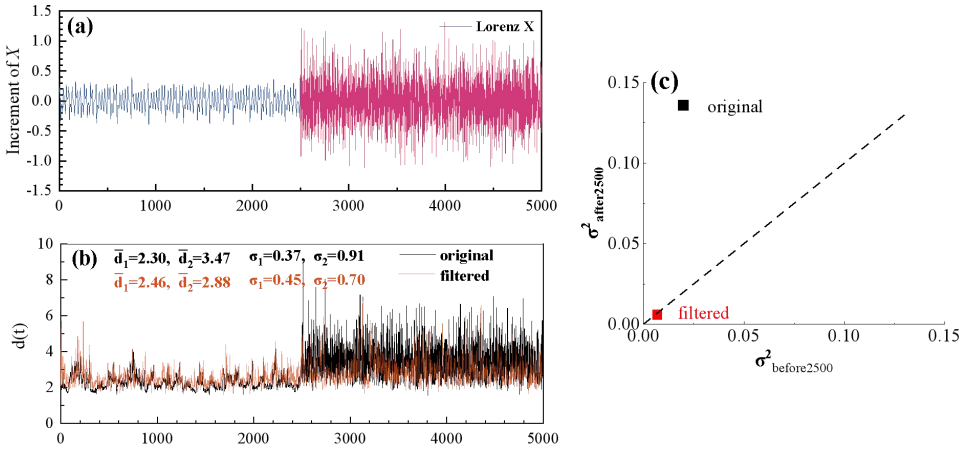

Figure 5: Results for *x* component of Lorenz-63 system with noise: the first half is noise-free and the second half (after 2500) with α=0.25 random noise. (a) The increment series: noise-free (blue) and with α=0.25 random noise (pink). (b) The evolution of calculated instantaneous dimension *d* for the original (black) and 30-step low-pass filtered (orange). (c) The scatter plot of variance of increment series before and after 2500 for the original (black) and 30-step low-pass filtered. Shifts for both DSID and increment are significant at the level of 0.001 from moving block bootstrap (MBB) test for original data and filtered data.

The dominated contribution of high-frequency variability on the SMV of DSID in SSTA can be also validated in the idealized models. For Lorenz systems, when the measurement noise strong enough, there will be a SMV of DSID (Fig. 3a and 3c). For example, when the noise strength is α=0.25 (Fig. 5a) for Lorenz-63 system, a SMV of DSID takes place with the mean value of DSID before and after the breaking point of 2500 changing from 2.30 to 3.47 (Fig. 5b). This marked transition almost disappears after the 30-step low-pass filtering (Fig. 5b) with the variances changing from large departing to on the one-to-one diagonal line (Fig. 5c). Similar behaviors can also be revealed in the high-dimensional Lorenz-96 system, and filtering works even better for the high-dimensional Lorenz-96 system than for the low-dimensional Lorenz-63 system (Fig. 6). And when the similar filtering is employed to case of the Lorenz-63 system under intermittent chaotic state shown in Fig. 3b, the SMV of DSID cannot be weaken considerably (Figure not shown here). All these results confirm the vital role of high-frequency variability in inducing the marked SMV of DSID in SSTA over some of the tropical Pacific regions.

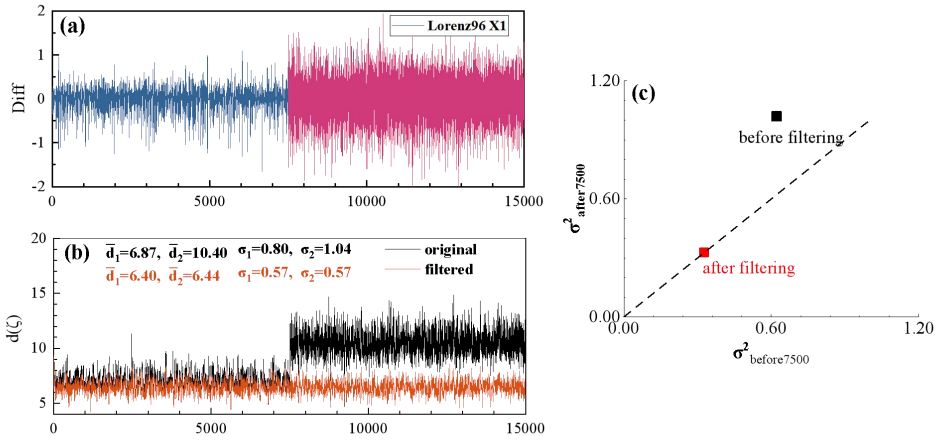

Figure 6: Results for *x* component of Lorenz-96 system with noise: the first half is noise-free and the second half (after 7500) with α=0.30 random noise. (a) The increment series: noise-free (blue) and with α=0.30 random noise (pink). (b) The evolution of calculated instantaneous dimension *d* for the original (black) and 10-step low-pass filtered (orange). (c) The scatter plot of variance of increment series before and after 7500 for the original (black) and 10-step low-pass filtered. Shifts for both DSID and increment are significant at the level of 0.001 from moving block bootstrap (MBB) test for original data, but not significant for filtered data.

4.3 Potential impacts of SSTA high-frequency variability difference over tropical Pacific

The high-frequency variability difference found in the tropical Pacific SSTA may have important implications for wide fields in climate research. The high-frequency variability is a fundamental aspect of weather and climate (Karl et al, 1995; Thompson et al, 2009). Many leading topics in weather and climate fields are closely related to and heavily rely on these high-frequency variability (Madden and Julian, 1971; Karl et al, 1995; Kämpf et al, 2004; Thompson et al, 2009; Lima and Wethey, 2012; Frolicher and Laufkotter, 2108; Oliver et al, 2018; Holbrook et al, 2019; Li et al, 2020; Ma et al, 2020; Strobach et al, 2020; Girishkumar et al, 2021; Hu et al, 2021; Huang et al, 2021; Huang et al, 2022a). For example, the trend estimation of high-frequency variability may be biased when there exists the variance shift of high-frequency variability over two periods (Karl et al, 1995). Three-to-six-day air-sea oscillation (Strobach et al, 2020) may be weaken when the high-frequency variability of SSTA is different over two periods. Atmospheric cold pools (Girishkumar et al, 2021) and tropical cyclone's cold wakes (Ma et al, 2020) induced intense rapid variations in SSTA may be masked by the variance shift of high-frequency variability over two periods. Moreover, the short-lasting intense MHW and its trend estimation (Lima and Wethey, 2012; Frolicher and Laufkotter, 2108; Oliver et al, 2018; Holbrook et al, 2019) may also be biased by the existence of shift in the high-frequency variability.

4 Discussions and Conclusions

It is found that there exists a marked SMV in the DSID from SSTA field over some tropical Pacific regions, especially the regions close to Maritime Continent and the Western Pacific warm pool, where the warm SST is mostly favorable to the anomalous convection to link the weather and climate over the tropics and extra-tropics (Huang et al 2021). This SMV in the DSID may be mainly caused by the high-frequency variability difference over different spans. The filtering test and the identical results obtained in the ideal Lorenz system, as well as the phenomenon of region dependence in the SMV, can all jointly support this viewpoint. If SMV originates from large-scale climate transitions, such as the state transition of the Pacific Decadal Oscillation (PDO), its impact should be spatially consistent. However, we found that SMV is more significant in the tropical central-western Pacific region. This regional dependence characteristic is incompatible with the attribution of large-scale climate transitions. The physical or non-physical mechanism that causes this SMV in the high-frequency variability of SSTA and its region-dependence is still unclear now. The drop in high-frequency variance in global-mean land temperature data in 1940s has been attributed to the incomplete spatial coverage of the station network and the decline in sampling variability during the late 1940s (Thompson et al, 2009). Similarly, this can also be taken as a possible reason for the shift in the high-frequency variability of SSTA over some tropical Pacific regions since it has been found that sparse satellite data might introduce artificial noise in OISST analyses (Reynolds et al, 2007; Banzon et al, 2016; Hu et al, 2021). Most importantly, it was documented that the input data sets to the daily OISST version 2 were changed from reprocessed or higher-quality data sets to operational data sets around the year of 2007 (Banzon et al, 2016), and the time changing the input data sets is consistent with the breaking point found in this study. However, the SMV strength of DSID is considerably different over different regions and there is a marked region-dependence in SMV strength of DSID (Fig. 1), which cannot be solely explained by the measurement operational changes and there must be more physical mechanisms unrevealed. More in-depth work along this line is still required in this field.

The shifts in the high-frequency variability of SSTA over some tropical Pacific regions are well characterized by the dynamical systems method with its instantaneous dimension. And it should be pointed out that even we calculate the DSID separately before and after the break point of shifts, the marked region-dependence in SMV strength of DSID found in Fig.1 is unchanged. Falasca and Bracco(2022) applied the same methodology over the entire tropical Pacific domain (20°S–20°N, 120°E–70°W) and failed to detect a significant mean decrease of DSID. This may be attributable to the choice of a larger research region and the multivariate approach, which together mask the structural change in the high-frequency variability of SSTA over the tropical central–western Pacific. It indicate that, when applying DSID to diagnose climate data, a refined regional analysis is more effective than a global aggregation in capturing regionally distinct variations in dynamical properties. The DSID can track the instantaneous variations of the SSTA field, and it can capture not only the shift related to the high-frequency variability of SSTA but also the transition to SSTA extreme states related to the changing of system states or controlling parameters. Since the changes of both the high-frequency variability and system controlling parameters are common things in the real-world systems, findings in this study can be easily extended to these systems and fields. At the

same time, duo to the sensitivity of the DSID to the noise and high-frequency variability, the shift found in DSID over different intervals can be employed to detect the consistence and homogenous of used data sets over different periods.

Author contributions

Ming Shi: Formal analysis; investigation; visualization; writing – review and editing. **Yu Huang:** Formal analysis; software; writing – review and editing. **Zuntao Fu:**Funding acquisition; project administration; supervision; writing – original draft; writing – review and editing. **Hao Xue**: writing – review and editing. **Xiaolong Qiu**: writing – review and editing. **Xintong Hao**: writing – review and editing. **Xiaohan Zhang**: writing – review and editing. **Haiyang Yu:** writing – review and editing. **Weiqi Xing**: writing – review and editing.

Acknowledgements

We acknowledge OISST v2.1 data are available at NOAA/NCEI (https://www.ncdc.noaa.gov/oisst/optimum-interpolation-sea-surface-temperature-oisst-v21).

Financial support

This research was supported in part by the National Key Research and Development Program of China (Grant No.2022YFB4202103), in part by the National Natural Science Foundation of China (Grant No.41975059), in part by the Science and Technology Project of China Huaneng Group (Grant No.HNKJ25-H06), and in part by the Foundation of Huaneng Clean Energy Research Institute (Grant No. TK-25-CERI02).

References

Ashok, K., Behera, S. K., Rao, S. A., Weng, H., and Yamagata, T.: El Niño Modoki and its possible teleconnection, Journal of Geophysical Research: Oceans, 112, https://doi.org/10.1029/2006JC003798, 2007.

Banzon, V., Smith, T. M., Chin, T. M., Liu, C., and Hankins, W.: A long-term record of blended satellite and in situ sea-surface temperature for climate monitoring, modeling and environmental studies, Earth System Science Data, 8, 165–176, https://doi.org/10.5194/essd-8-165-2016, 2016.

Borghezan, M. and Rech, P. C.: Chaos and periodicity in Vallis model for El Niño, Chaos, Solitons & Fractals, 97, 15–18, https://doi.org/10.1016/j.chaos.2017.01.018, 2017.

Carlstein, E.: The use of subseries values for estimating the variance of a general statistic from a stationary sequence, Ann. Statist., 14, 1171–1179, https://doi.org/10.1214/aos/1176350057, 1986.

Datseris, G., Kottlarz, I., Braun, A. P., and Parlitz, U.: Estimating fractal dimensions: A comparative review and open source implementations, Chaos: An Interdisciplinary Journal of Nonlinear Science, 33(10), https://doi.org/10.1063/5.0160394, 2023.

Deser, C. and Blackmon, M. L.: Surface Climate Variations over the North Atlantic Ocean during Winter: 1900–1989, Journal of Climate, 6, 1743–1753, https://doi.org/10.1175/1520-0442(1993)006%253C1743:SCVOTN%253E2.0.CO;2, 1993.

Ding, R. and Li, J.: Nonlinear finite-time Lyapunov exponent and predictability, Physics Letters A, 364, 396–400, https://doi.org/10.1016/j.physleta.2006.11.094, 2007.

Ding, R., Li, J., Zheng, F., Feng, J., and Liu, D.: Estimating the limit of decadal-scale climate predictability using observational data, Climate Dynamics, 46, 1563–1580, https://doi.org/10.1007/s00382-015-2662-6, 2015.

Dong, C., Faranda, D., Gualandi, A., Lucarini, V., and Mengaldo, G.: Time-lagged recurrence: A data-driven method to estimate the predictability of dynamical systems, Proceedings of the National Academy of Sciences, 122, e2420252122, https://doi.org/10.1073/pnas.2420252122, 2025.

Efron, B.: Bootstrap methods: another look at the jackknife, in Breakthroughs in Statistics: Methodology and Distribution, 569–593, https://doi.org/10.1007/978-1-4612-4380-9_41, 1992.

Falasca, F. and Bracco, A.: Exploring the tropical Pacific manifold in models and observations, Physical Review X, 12, 021054, https://doi.org/10.1103/PhysRevX.12.021054, 2022.

Fan, M. and Schneider, E. K.: Observed Decadal North Atlantic Tripole SST Variability. Part I: Weather Noise Forcing and Coupled Response, Journal of the Atmospheric Sciences, 69, 35–50, https://doi.org/10.1175/JAS-D-11-018.1, 2012.

Faranda, D. and Vaienti, S.: Extreme value laws for dynamical systems under observational noise, Physica D: Nonlinear Phenomena, 280–281, 86–94, https://doi.org/10.1016/j.physd.2014.04.011, 2014.

Faranda, D., Freitas, J. M., Lucarini, V., Turchetti, G., and Vaienti, S.: Extreme value statistics for dynamical systems with noise, Nonlinearity, 26, 2597, https://doi.org/10.1088/0951-7715/26/9/2597, 2013.

Faranda, D., Freitas, J.M., Guiraud, P., Vaienti, S.: Extreme value theory for piecewise contracting maps with randomly applied stochastic perturbations. Stochastics Dynamics 16, 1660015, https://doi.org/10.1142/S0219493716600157, 2016.

Faranda, D., Messori, G., Alvarez-Castro, M. C., and Yiou, P.: Dynamical properties and extremes of Northern Hemisphere climate fields over the past 60 years, Nonlinear Processes in Geophysics, 24, 713–725, https://doi.org/10.5194/npg-24-713-2017, 2017a.

Faranda, D., Messori, G., and Yiou, P.: Dynamical proxies of North Atlantic predictability and extremes, Sci Rep, 7, 41278, https://doi.org/10.1038/srep41278, 2017b.

Faranda, D., Alvarez-Castro, M. C., Messori, G., Rodrigues, D., and Yiou, P.: The hammam effect or how a warm ocean enhances large scale atmospheric predictability, Nat Commun, 10, 1316, https://doi.org/10.1038/s41467-019-09305-8, 2019.

Faranda, D., Messori, G., and Yiou, P.: Diagnosing concurrent drivers of weather extremes: application to warm and cold days in North America, Clim Dyn, 54, 2187–2201, https://doi.org/10.1007/s00382-019-05106-3, 2020.

Faranda, D., Sato, Y., Dong, C., Gualandi, A., Noyelle, R., Alberti, T., Dubrulle, B., Fery, L., Messori, G., Vrac, M., et al.: El Niño and droughts in Southeast Asia: A stochastic-chaotic modeling approach, Physical Review E, 111, 064209, https://doi.org/10.1103/PhysRevE.111.064209, 2025.

Feng, J., Ding, R., Liu, D., and Li, J.: The application of nonlinear local Lyapunov vectors to ensemble predictions in Lorenz systems, Journal of the Atmospheric Sciences, 71, 3554–3567, https://doi.org/10.1175/JAS-D-13-0270.1, 2014.

Feng, J., Li, J., Ding, R., and Toth, Z.: Comparison of nonlinear local Lyapunov vectors and bred vectors in estimating the spatial distribution of error growth, Journal of the Atmospheric Sciences, 75, 1073–1087, https://doi.org/10.1175/JAS-D-17-0266.1, 2018.

Frölicher, T. L. and Laufkötter, C.: Emerging risks from marine heat waves, Nat Commun, 9, 650, https://doi.org/10.1038/s41467-018-03163-6, 2018.

Garay, B. M. and Indig, B.: Chaos in Vallis' asymmetric Lorenz model for *El Niño*, Chaos, Solitons & Fractals, 75, 253–262, https://doi.org/10.1016/j.chaos.2015.02.015, 2015.

Girishkumar, M. S., Joseph, J., McPhaden, M. J., and Pattabhi Ram Rao, E.: Atmospheric Cold Pools and Their Influence on Sea Surface Temperature in the Bay of Bengal, Journal of Geophysical Research: Oceans, 126, e2021JC017297, https://doi.org/10.1029/2021JC017297, 2021.

Guo, Y., Huang, Y., and Fu, Z.: Regional compound humidity-heat extremes in the mid-lower reaches of the Yangtze River: a dynamical systems perspective, Environ. Res. Lett., 17, 064032, https://doi.org/10.1088/1748-9326/ac715f, 2022.

Hall, P.: Resampling a coverage pattern, Stochastic Process. Appl., 20, 231–246, https://doi.org/10.1016/0304-4149(85)90217-6, 1985.

Hall, P., Horowitz, J. L., and Jing, B.-Y.: On blocking rules for the bootstrap with dependent data, Biometrika, 82, 561–574, https://doi.org/10.1093/biomet/82.3.561, 1995.

He, W., Xie, X., Mei, Y., Wan, S., and Zhao, S.: Decreasing predictability as a precursor indicator for abrupt climate change, Climate Dynamics, 56, 3899–3908, https://doi.org/10.1007/s00382-021-05676-1, 2021.

Holbrook, N. J., Scannell, H. A., Sen Gupta, A., Benthuysen, J. A., Feng, M., Oliver, E. C. J., Alexander, L. V., Burrows, M. T., Donat, M. G., Hobday, A. J., Moore, P. J., Perkins-Kirkpatrick, S. E., Smale, D. A., Straub, S. C., and Wernberg, T.: A global assessment of marine heatwaves and their drivers, Nat Commun, 10, 2624, https://doi.org/10.1038/s41467-019-10206-z, 2019.

Hou, Z., Li, J., Ding, R., Karamperidou, C., Duan, W., Liu, T., and Feng, J.: Asymmetry of the predictability limit of the warm ENSO phase, Geophysical Research Letters, 45, 7646–7653, https://doi.org/10.1029/2018GL077880, 2018.

Hou, Z., Li, J., Ding, R., and Feng, J.: Investigating decadal variations of the seasonal predictability limit of sea surface temperature in the tropical Pacific, Climate Dynamics, 2022, 1–18, https://wgmktpgxscrjl-s.p.lib.tju.edu.cn/10.1007/s00382-022-06179-3, 2022.

Hu, Y., Beggs, H., and Wang, X. H.: Intercomparison of High-Resolution SST Climatologies Over the Australian Region, Journal of Geophysical Research: Oceans, 126, e2021JC017221, https://doi.org/10.1029/2021JC017221, 2021.

Huang, Y. and Fu, Z.: Enhanced time series predictability with well-defined structures, Theor Appl Climatol, 138, 373–385, https://doi.org/10.1007/s00704-019-02836-6, 2019.

Huang, Y., Fu, Z., and Franzke, C. L. E.: A Secular Shift of the Madden-Julian Oscillation and Its Relation to Western Pacific Ocean Warming, Geophysical Research Letters, 48, e2021GL095400, https://doi.org/10.1029/2021GL095400, 2021.

Huang, Y., Shi, M., and Fu, Z.: A Dynamical Systems Perspective to Characterize the El Niño Diversity in Spatiotemporal Patterns, Front. Phys., 10, https://doi.org/10.3389/fphy.2022.919951, 2022a.

Huang, Y., Yuan, N., Shi, M., Lu, Z., and Fu, Z.: On the Air-Sea Couplings Over Tropical Pacific: An Instantaneous Coupling Index Using Dynamical Systems Metrics, Geophysical Research Letters, 49, e2021GL097049, https://doi.org/10.1029/2021GL097049, 2022b.

Jeong, H.-I. and Ahn, J.-B.: A new method to classify ENSO events into eastern and central Pacific types, International Journal of Climatology, 37, 2193–2199, https://doi.org/10.1002/joc.4813, 2017.

Jin, F.-F., Neelin, J. D., and Ghil, M.: El Niño on the Devil's Staircase: Annual Subharmonic Steps to Chaos, Science, 264, 70–72, https://doi.org/10.1126/science.264.5155.70, 1994.

Kämpf, J., Doubell, M., Griffin, D., Matthews, R. L., and Ward, T. M.: Evidence of a large seasonal coastal upwelling system along the southern shelf of Australia, Geophysical Research Letters, 31, https://doi.org/10.1029/2003GL019221, 2004.

Kao, H.-Y. and Yu, J.-Y.: Contrasting Eastern-Pacific and Central-Pacific Types of ENSO, Journal of Climate, 22, 615–632, https://doi.org/10.1175/2008JCLI2309.1, 2009.

Karl, T. R., Knight, R. W., and Plummer, N.: Trends in high-frequency climate variability in the twentieth century, Nature, 377, 217–220, https://doi.org/10.1038/377217a0, 1995.

Kug, J.-S., Jin, F.-F., and An, S.-I.: Two Types of El Niño Events: Cold Tongue El Niño and Warm Pool El Niño, Journal of Climate, 22, 1499–1515, https://doi.org/10.1175/2008JCLI2624.1, 2009.

Künsch, H. R.: The jackknife and the bootstrap for general stationary observations, Ann. Statist., 17, 1217 – 1241, https://doi.org/10.1214/aos/1176347265, 1989.

Kushnir, Y.: Interdecadal Variations in North Atlantic Sea Surface Temperature and Associated Atmospheric Conditions, Journal of Climate, 7, 141–157, https://doi.org/10.1175/1520-0442(1994)007%253C0141:IVINAS%253E2.0.CO;2, 1994.

Li, J. and Ding, R.: Temporal – Spatial Distribution of Atmospheric Predictability Limit by Local Dynamical Analogs, Monthly Weather Review, 139, 3265–3283, https://doi.org/10.1175/MWR-D-10-05020.1, 2011.

Li, J., Feng, J., and Ding, R.: Attractor radius and global attractor radius and their application to the quantification of predictability limits, Climate Dynamics, 51, 2359–2374, https://doi.org/10.1007/s00382-017-4017-y, 2017.

Li, X., Ding, R., and Li, J.: Determination of the backward predictability limit and its relationship with the forward predictability limit, Advances in Atmospheric Sciences, 36, 669–677, https://doi.org/10.1007/s00376-019-8205-z, 2019.

Li, X., Ding, R., and Li, J.: Quantitative study of the relative effects of initial condition and model uncertainties on local predictability in a nonlinear dynamical system, Chaos, Solitons & Fractals, 139, 110094, https://doi.org/10.1016/j.chaos.2020.110094, 2020.

Li, X. and Ding, R.: The backward nonlinear local Lyapunov exponent and its application to quantifying the local predictability of extreme high-temperature events, Climate Dynamics, 60, 2767–2781, https://doi.org/10.1007/s00382-022-06469-w, 2023.

Li, X., Ding, R., and Li, J.: The BaSIC method: a new approach to quantitatively assessing the local predictability of extreme weather events, Climate Dynamics, 60, 3561–3576, https://doi.org/10.1007/s00382-022-06526-4, 2023.

Lima, F. P. and Wethey, D. S.: Three decades of high-resolution coastal sea surface temperatures reveal more than warming, Nat Commun, 3, 704, https://doi.org/10.1038/ncomms1713, 2012.

Lorenz, E.N.: Deterministic nonperiodic flow. Journal of the Atmospheric Sciences 20, 130-411, https://doi.org/10.1177/0309133308091948, 1963

Lorenz, E. N.: Predictability – a problem partly solved, in: Predictability of Weather and Climate, edited by: Hagedorn, R. and Palmer, T., Cambridge University Press, Cambridge, 40–58, https://doi.org/10.1017/CBO9780511617652.004, 2006

Luca, P.D., Messori, G., Faranda, D., Ward, P. J., and Coumou, D.: Compound warm–dry and cold–wet events over the Mediterranean, Earth System Dynamics, 11, 793–805, https://doi.org/10.5194/esd-11-793-2020, 2020a.

Luca, P.D., Messori, G., Pons, F. M. E., and Faranda, D.: Dynamical systems theory sheds new light on compound climate extremes in Europe and Eastern North America, Quarterly Journal of the Royal Meteorological Society, 146, 1636–1650, https://doi.org/10.1002/qj.3757, 2020b.

Lucarini, V., Faranda, D., and Wouters, J.: Universal Behaviour of Extreme Value Statistics for Selected Observables of Dynamical Systems, J Stat Phys, 147, 63–73, https://doi.org/10.1007/s10955-012-0468-z, 2012.

Ma, Z., Fei, J., Lin, Y., and Huang, X.: Modulation of Clouds and Rainfall by Tropical Cyclone's Cold Wakes, Geophysical Research Letters, 47, e2020GL088873, https://doi.org/10.1029/2020GL088873, 2020.

Madden, R. A. and Julian, P. R.: Detection of a 40–50 Day Oscillation in the Zonal Wind in the Tropical Pacific, Journal of the Atmospheric Sciences, 28, 702–708, https://doi.org/10.1175/1520-0469(1971)028%253C0702:DOADOI%253E2.0.CO;2, 1971.

Manneville, P. and Pomeau, Y.: Intermittency and the Lorenz model, Physics Letters A - PHYS LETT A, 75, 1–2, https://doi.org/10.1016/0375-9601(79)90255-X, 1979.

Manneville, P. and Pomeau, Y.: Different ways to turbulence in dissipative dynamical systems, Physica D: Nonlinear Phenomena, 1, 219–226, https://doi.org/10.1016/0167-2789(80)90013-5, 1980.

Messori, G., Caballero, R., and Faranda, D.: A dynamical systems approach to studying midlatitude weather extremes, Geophysical Research Letters, 44, 3346–3354, https://doi.org/10.1002/2017GL072879, 2017.

Oliver, E. C. J., Donat, M. G., Burrows, M. T., Moore, P. J., Smale, D. A., Alexander, L. V., Benthuysen, J. A., Feng, M., Sen Gupta, A., Hobday, A. J., Holbrook, N. J., Perkins-Kirkpatrick, S. E., Scannell, H. A., Straub, S. C., and Wernberg, T.: Longer and more frequent marine heatwaves over the past century, Nat Commun, 9, 1324, https://doi.org/10.1038/s41467-018-03732-9, 2018.

Politis, D. N., and Romano, J. P.: The stationary bootstrap, J. Amer. Statist. Assoc., 89, 1303 – 1313, https://doi.org/10.1080/01621459.1994.10476870, 1994.

Reynolds, R. W., Smith, T. M., Liu, C., Chelton, D. B., Casey, K. S., and Schlax, M. G.: Daily High-Resolution-Blended Analyses for Sea Surface Temperature, Journal of Climate, 20, 5473–5496, https://doi.org/10.1175/2007JCLI1824.1, 2007.

Schreiber, T., and Schmitz, A.: Surrogate time series, Physica D, 142, 346 – 382, https://doi.org/10.1016/S0167-2789(00)00043-9, 2000.

Shi, M., Huang, Y., and Fu, Z.: Dynamical systems persistence parameter of sea surface temperature and its associations with regional averaged index over the tropical Pacific, International Journal of Climatology, 42, 7550–7562, https://doi.org/10.1002/joc.7664, 2022.

Small, M., and Tse, C.K.: Applying the method of surrogate data to cyclic time series, Physica D, 164, 187 – 201, https://doi.org/10.1016/S0167-2789(02)00382-2, 2002.

Strobach, E., Molod, A., Trayanov, A., Forget, G., Campin, J.-M., Hill, C., and Menemenlis, D.: Three-to-Six-Day Air–Sea Oscillation in Models and Observations, Geophysical Research Letters, 47, e2019GL085837, https://doi.org/10.1029/2019GL085837, 2020.

Sun, Y., Han, L., Li, J.P., Ding, R.Q.: Dynamic properties of sea level pressure field in east Asia-northwest Pacific, Chinese Journal of Atmospheric Sciences 46(1), 70-82, 2022. (in Chinese)

Theiler, J., Eubank, S., Longtin, A., Galdrikian, B., and Farmer, J.D.: Testing for nonlinearity in time series: the method of surrogate data, Physica D, 58, 77–94, https://doi.org/10.1016/0167-2789(92)90102-S, 1992.

Thompson, D. W. J., Wallace, J. M., Jones, P. D., and Kennedy, J. J.: Identifying Signatures of Natural Climate Variability in Time Series of Global-Mean Surface Temperature: Methodology and Insights, Journal of Climate, 22, 6120–6141, https://doi.org/10.1175/2009JCLI3089.1, 2009.

Trenberth, K. E. and Stepaniak, D. P.: Indices of El Niño Evolution, Journal of Climate, 14, 1697–1701, https://doi.org/10.1175/1520-0442(2001)014%253C1697:LIOENO%253E2.0.CO;2, 2001.

Tziperman, E., Stone, L., Cane, M. A., and Jarosh, H.: El Niño Chaos: Overlapping of Resonances Between the Seasonal Cycle and the Pacific Ocean-Atmosphere Oscillator, Science, 264, 72–74, https://doi.org/10.1126/science.264.5155.72, 1994.

Vallis, G. K.: El Niño: A Chaotic Dynamical System?, Science, 232, 243–245, https://doi.org/10.1126/science.232.4747.243, 1986.

Vallis, G. K.: Conceptual models of El Niño and the Southern Oscillation, Journal of Geophysical Research: Oceans, 93, 13979–13991, https://doi.org/10.1029/JC093iC11p13979, 1988.

Wu, L. and Liu, Z.: North Atlantic Decadal Variability: Air–Sea Coupling, Oceanic Memory, and Potential Northern Hemisphere Resonance, Journal of Climate, 18, 331–349, https://doi.org/10.1175/JCLI-3264.1, 2005.